The GERB Edition 1 products SEVIRI scene identification

Alessandro Ipe[ab], Cédric Bertrand[a], Nicolas Clerbaux[ab], Steven Dewitte[a] and Luis Gonzalez[a]

[a]Royal Meteorological Institute of Belgium, Brussels, Belgium;
[b]Vrije Universiteit Brussel, Brussels, Belgium

ABSTRACT

The first Geostationary Earth Radiation Budget (GERB) instrument was launched during the 2002 summer together with the Spinning Enhanced Visible and InfraRed Imager (SEVIRI) on board of the Meteosat-8 satellite. This broadband radiometer aims to deliver near real-time estimates of the top of the atmosphere solar and thermal radiative fluxes at high temporal resolution thanks to the geostationary orbit. Such goal is achieved with the L20 GERB processing which generates these fluxes at several spatial resolutions from the directional filtered radiance measurements of the instrument. This processing consists of successive components, one of them being a radiance-to-flux conversion. Such conversion is carried out in the solar region by using the shortwave angular dependency models (ADMs) developed from the Tropical Rainfall Measuring Mission (TRMM) Clouds and the Earth's Radiant Energy System (CERES) experiment. As these ADMs are stratified according to specific scene properties, the GERB ground segment will have to rely on a scene identification of SEVIRI data which allows us to select the proper ADM.

In this paper, we will briefly justify and describe the implementation of a specific GERB scene identification for the official Edition 1 release of the L2 products. Preliminary comparisons between GERB and CERES scene identifications both applied to SEVIRI data will follow. Finally, we will suggest possible improvements based on limitations which could be found.

Keywords: remote sensing, Earth radiation budget, narrowband imager, scene identification, visible wavelengths, cloud properties retrievals

1. INTRODUCTION

The Geostationary Earth Radiation Budget (GERB) instruments which are/will be the co–passengers of the Spinning Enhanced Visible and InfraRed Imagers on board of the Meteosat Second Generation (MSG) satellites' constellation[1] are broadband radiometers measuring the outgoing radiation of the Earth–atmosphere system in a shortwave and a totalwave channel every 5 minutes 30 seconds. Based on such measurements, the aim of the GERB project[2,3] is to deliver on a near realtime basis top–of–the–atmosphere (TOA) solar and thermal fluxes to the science community with a target accuracy of about 5 Wm^{-2} every 15 minutes. Such a goal is achieved by the synergetic use of SEVIRI data within the Royal Meteorological Institute of Belgium (RMIB) GERB Processing (RGP). This processing consists to apply successively a spectral modeling, a radiance–to–flux conversion and a resolution enhancement of the products at a higher spatial resolution (typically 10 km) than the native GERB instrument sampling (about 45 km at nadir).[4] The figure 1 gives an overview of the general scheme of the processing.

The radiance–to-flux conversion scheme of the RGP relies on the use of implicit (thermal)[5,6] and explicit (solar) angular dependency models (ADMs). For the solar fluxes, the Clouds and Earth's Radiant Energy System (CERES)[7] Tropical Rainfall Monitoring Mission (TRMM)[8] ADMs[9] relates the unfiltered radiances to the fluxes through multiplicative factors according to specific scene type properties (physic and geometric) which are derived by a scene identification. Even if the CERES scene identification is a complex iterative scheme providing quantitative estimates of numerous atmospheric and surface parameters mainly based on the Visible

Further author information: (Send correspondence to A.I.)
A.I.: E-mail: Alessandro.Ipe@oma.be, Telephone: +32 2 373 0631, Fax: +32 2 374 6788, Address: Royal Meteorological Institute of Belgium (RMIB), Department of Observations, Section Remote Sensing from Space, Avenue Circulaire 3, 1180 Brussels, Belgium

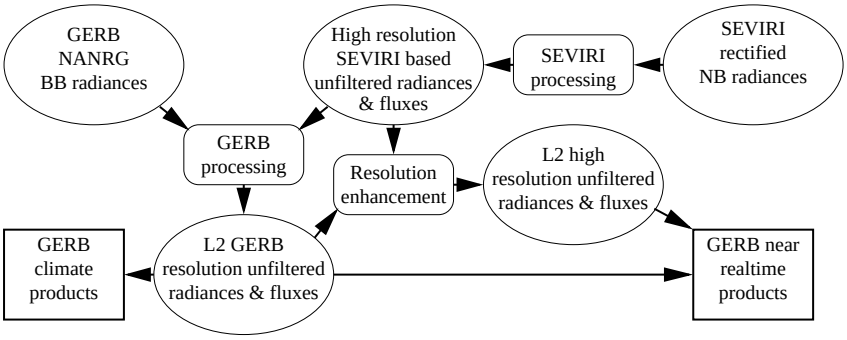

Figure 1. Overview of the RMIB GERB Processing.

Infrared Solar-Infrared Split Window Technique (VISST) algorithm,[10,11] it was shown that the ADMs need only to be stratified according to 4 features–surface geotype, cloud thermodynamic phase, cloud optical depth and cloud fraction– over the CERES footprint (about 10 km at nadir) to reach satisfactory accuracy.[12]

Therefore, due to limited available resources and to the near realtime constraint (each repeat cycle must be processed within 15 minutes), adapting the VISST method to SEVIRI was not feasible for the RGP. Instead, we decided to develop and implement a simple but robust cloud properties retrieval scheme giving similar results than the CERES algorithm for the 4 features used to characterize the ADMs.

In the following section, we will briefly describe the algorithm which was developed for the RGP and give examples of its output. Then, in section 3, we will discuss the results of our comparisons between the GERB and CERES scene identifications. Finally, we will conclude and suggest issues to address and future work to possibly improve the matching between the two schemes.

2. ALGORITHM

The method used in the RGP is extensively described in 13. Thus we will only give a brief description in the following.

The strategy which was adopted for the design of this scene identification is non–iterative. It consists to apply for every SEVIRI pixel the successive steps:

1. assign the surface geotype according to a static surface type map (identical to CERES),[9,14]
2. infer the potential cloud thermodynamic phase using a fixed threshold of 255 K on the SEVIRI 10.8 μm brightness temperature,[15]
3. using the reflectance associated to the channel with the highest cloud/clearsky dynamic between the 0.6 and 0.8 μm visible bands, derive the cloud optical depth through comparisons with an a priori reference composite TOA clearsky reflectance (see section 2.1) and lookup tables from 1D radiative transfer model (RTM) computations,[16]
4. assign a cloudy/non–cloudy flag from a threshold test on the cloud optical depth.

Finally, these features are averaged to 3×3 SEVIRI pixels (about 10 km) which is the input resolution of the SEVIRI RGP processing and the native CERES resolution used to derive the ADMs and compute the cloud fraction over such footprint.

2.1 Composite TOA clearsky visible reflectances

These reference images are computed for each repeat cycle of the day, i.e. every 15 minutes. However, they are only updated once a week due to computing constraints. Basically, for every pixel, visible channel and time of the day, a clearsky reflectance is estimated by using a curve–driven percentile approach on the reflectance time–series over a given time period. Nevertheless, even if this method is almost insensitive to cloud shadows, it was improved to be more robust to surface changes occurring in only several days (mainly over tundra vegetation). However, for the geostationary orbit, this method is not valid anymore within regions affected by the sunglint. This is due to the fact that it is a daily transient phenomenon modifying locally the ocean reflectance to extreme values. Due to their extensive areas, we cannot adopt the common approach found in the literature which simply consists to flag such regions as invalid. Thus, cloud properties still need to be derived even with lowest accuracy. Therefore, in these regions, we are currently using a coarse parameterization of the clearsky ocean reflectance according to 1D RTM simulations (based on DISORT and the Cox–Munk surface model).[17,18] Figure 2 illustrates the result of this scheme in a false color composition.

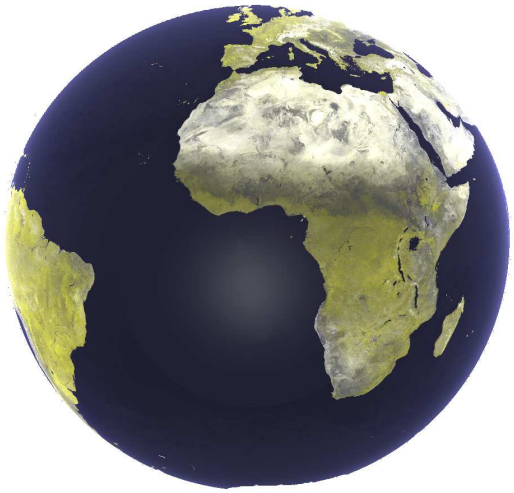

Figure 2. False color composite visible clearsky image for January 17 2006 at 12:00 GMT (red: 0.8 μm, green: 0.6 μm and blue: 0.6 μm).

2.2 Cloud optical depth retrievals

The strategy selected here is similar to 19 which consists of using lookup tables (LUTs) of precomputed values of TOA reflectances according to various scene geometries, atmospheric conditions and surface types. These tables were generated using the STREAMER[16] RTM for a limited set of ideal scenes (5 Lambertian surfaces, one uniform cloud layer for each thermodynamic phase) with several cloud optical depth τ values ranging from 0 to 128 as input. As shown in 20, there is an empirical relation between the reflectances and the cloud optical depth which is merely insensitive to cloud particle size in the visible wavelengths. By rescaling this law between 0 and 1 according to the mean cloud amount for each visible channel λ

$$C_\lambda(\theta_0,\theta,\varphi,\alpha,\text{phase},\tau) = \frac{\rho_\lambda(\theta_0,\theta,\varphi,\alpha,\text{phase},\tau) - \rho_\lambda(\theta_0,\theta,\varphi,\alpha,\tau=0)}{\rho_\lambda(\theta_0,\theta,\varphi,\text{phase},\tau=128) - \rho_\lambda(\theta_0,\theta,\varphi,\alpha,\tau=0)}$$

where, $\tau = 0$, represents clearsky conditions above the ground surface, $\tau = 128$ (for consistency with CERES), denotes the opposite boundary limit associated with optically opaque cloudy conditions leading to simulated radiance fields insensitive to surface type α, we have found that, due to the specific shape of these curves, the LUTs can be parameterized using a modified sigmoid function of the logarithm of the cloud optical depth (for more details, see 21). One can found in figure 3(c) the estimation of the cloud optical depth retrievals for a specific day and time of the SEVIRI field–of–view (FOV).

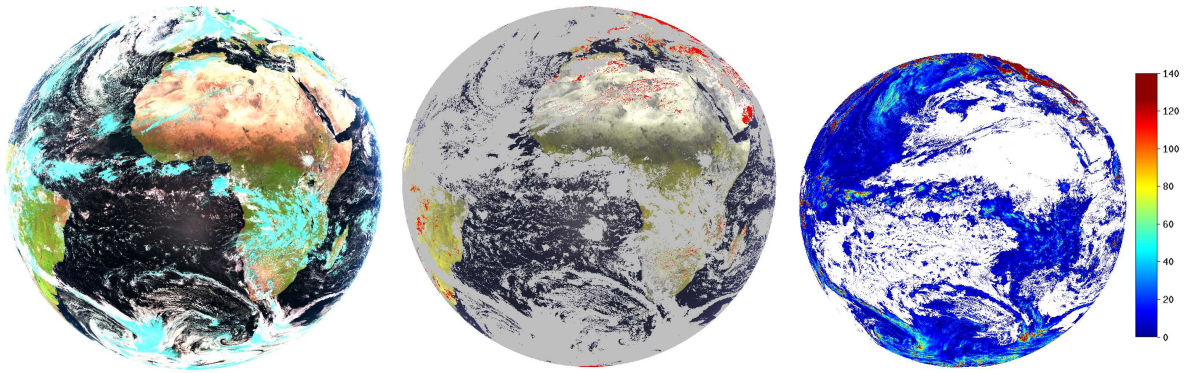

(a) (b) (c)

Figure 3. (a) False color visible reflectance image (red: 0.8 μm, green: 0.6 μm and blue: 0.6 μm), (b) cloud flag image (red designates no retrieval) and (c) cloud optical depth retrievals (white pixels designate clearsky areas) for January 17 2006 at 12:00 GMT.

Therefore, the retrieval scheme follows for every SEVIRI pixel:

1. select the visible channel associated to the largest denominator of the mean cloud amount for highest sensitivity using the composite clearsky and opaque RTM values (basically 0.8 μm for ocean and 0.6 μm for other surfaces),
2. for this channel, compute C and estimate the associated cloud optical depth using the reverse explicit parameterization of the LUTs according to the cloud phase (thanks to the sigmoid function).

2.3 Cloud flag

Instead of relying on multispectral tests like the major cloud detection algorithms found in the literature, we have decided to remain consistent with the cloud optical depth retrievals. Therefore, the RGP threshold test simply consists to flag a pixel as cloudy if its derived cloud optical depth is above some value (typically 0.6,[21] plus a 3×3 window variability term based on the composite clearsky reflectance values). The result of this test is given in figure 3(b). One can note that the regions affected with no retrieval are mostly associated with extreme viewing zenith angle conditions.

3. COMPARISONS

As mentioned earlier, the GERB scene identification was designed to only retrieve the features used to stratify the CERES TRMM solar ADMs which are then used in the radiance–to–flux conversion scheme in the RGP processing. Therefore, to avoid any systematic bias in the derived TOA fluxes, we need to mimic as close as possible the CERES scene identification retrievals for every footprint.

Previous comparisons were performed between overlapping Meteosat–7 and CERES Single Scan Footprint (SSF) data.[21] However, due to the difference between the satellites' platforms (geostationary and polar), an extensive search on collocated footprints had to be made. The difference between the spectral response of the imagers was also prone to errors.

As the CERES Cloud Working Group has adapted their scene identification algorithm to be directly run on SEVIRI data, comparisons between GERB and CERES retrievals will be eased even if the latter are still considered as preliminary by the CERES Cloud Working Group. Nevertheless, different calibrations used could still lead to discrepancies between the two schemes.

3.1 Data

These comparisons were performed on daytime data for 6–12 March 2007. GERB retrievals were generated with the Edition 1 RGP processing at the SEVIRI native resolution (3 km at nadir). CERES retrievals were generated with the SEVIRI VISST processing running at half the native SEVIRI resolution, i.e. 1 pixel out of 2, for what is called the ARM-NIAMEY and EUROPE windows (see `http://www-angler.larc.nasa.gov/satimage/products.html`). VISST data were then projected to the SEVIRI field–of–view (FOV) to allow direct one–to–one pixel comparisons as illustrated in figure 4. It can be shown that SEVIRI 0.6 μm reflectances used in the VISST processing are about 6 % higher that those obtained using EUMETSAT prescribed calibration which is applied in the RGP. Therefore, such difference in the calibrations used in the two schemes could explain part of the discrepancies between their retrievals. However, quantitative estimation of the implied errors is difficult to perform.

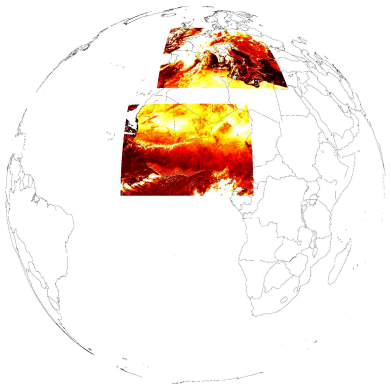

Figure 4. Reflectance image of the 0.6 μm SEVIRI band showing the domain used in the comparisons for January 17 2006 at 12:00 GMT.

3.2 Cloud flag

The overall statistics of the cloud flag comparisons for the dataset can be found in table 1 as a confusion matrix. One can see that the percentage of matching retrievals (cloudy and clearsky) is about 85 % (sum of the diagonal terms). Due to the limitation of the GERB cloud flag method, thin clouds with cloud optical depth below the selected threshold value of 0.6 will falsely be classified as clear compared to CERES. Thus it should increase the percentage of mismatches accordingly compared to the other mismatch scenario (GERB: cloudy and VISST: clear) while it is the opposite (see off–diagonal terms).

Table 1. Confusion matrix between GERB and CERES/VISST cloud flagging algorithms.

	VISST	
GERB	clear	cloudy
clear	53.39 %	3.53 %
cloudy	11.71 %	31.37 %

To investigate the discrepancies between the two methods, we have plotted in figure 5 the relative histograms of the cloud optical depth for both off-diagonal terms. In both cases, it implies scenes with broad range of cloud optical depth values and therefore, it suggests that the mismatches are not simply due to the simple thresholding technique used for GERB but instead to some combination of the differences between the calibrations, the clearsky reflectances (for GERB) and the surface albedos (for CERES) and/or the cloud optical depth LUTs (thus the radiative transfer models used to build them). However, further investigations will be needed to point out the dominant factor.

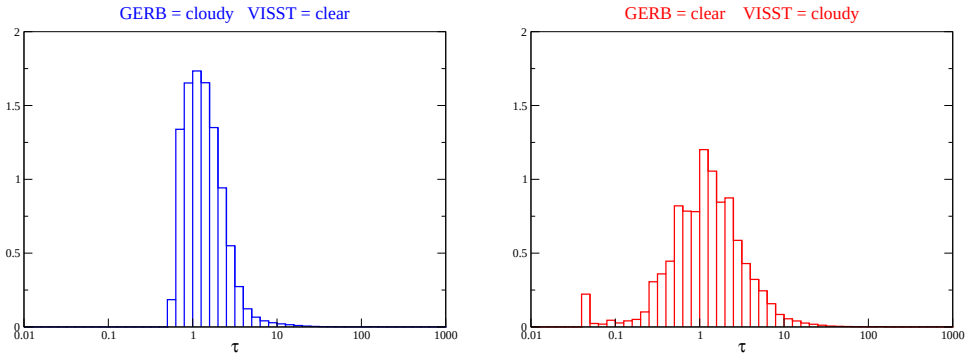

(a) (b)

Figure 5. Relative frequency histograms of cloud optical depth values for mismatched scenes according to GERB and CERES cloud flags.

3.3 Cloud phase

Table 2 gives the overall statistics of the cloud phase comparisons for the dataset. Similar matching (water and ice) between the two schemes occurs in about 75 % of the cases (sum of the diagonal terms). GERB is flagging 1.87 % of the scenes as ice while CERES is flagging them as water. This can be explained by the fact that the GERB method is only relying on a single threshold test on the brightness temperature of the SEVIRI 10.6 μm chanel compared to CERES and thus misclassifies clouds made by supercooled water droplets. On the opposite, the percentage of discrepancy for scenes flagged by GERB as water and CERES as ice is much higher (about 23 %). This could be due to the fact that the threshold brightness temperature of 255 K between water and ice clouds used in the RGP is too low. However, it could also be explained by misclassification of snow as ice clouds by the VISST scheme still being in a development stage at this point. Therefore, carefull investigations still need to be performed.

Table 2. Confusion matrix between GERB and CERES/VISST cloud phase algorithms.

GERB	VISST	
	water	ice
water	43.39 %	22.88 %
ice	1.87 %	31.87 %

3.4 Cloud optical depth

To compare the cloud optical depth retrievals from GERB and CERES/VISST algorithms, we have selected scenes where both are flagging them as cloudy with the same cloud phase. In figure 6 we have plotted the frequency histograms of the cloud optical depth according to each method for water and ice clouds as well as the correlation coefficient ρ. From both graphs, one can see the saturation of values at 128 which was taken as upper bound in the CERES scheme and thus also for GERB to be consistent. The main assumption is that the radiance field above optically thick overcast scenes is nearly independent of the cloud optical depth above such value. The limitation of the GERB algorithm for thin clouds detection is also obvious due to the GERB cut–off value of about 0.6 for the cloud flag test. Nevertheless, we can see that there is still good agreement between the retrievals according to the correlation coefficients. However, dark blue stripes can be observed in the histograms and this could suggest misselection of LUTs within the RGP for specific scenes mainly due to the fact that the surface map is fixed across the whole year and not taking into account of the seasonal change of vegetation.

4. CONCLUSIONS AND FUTURE WORKS

In this paper we have briefly described the scene identification algorithm used within the RGP processing for the Edition 1 L2 GERB data which are freely available to the scientific community. Preliminary comparisons

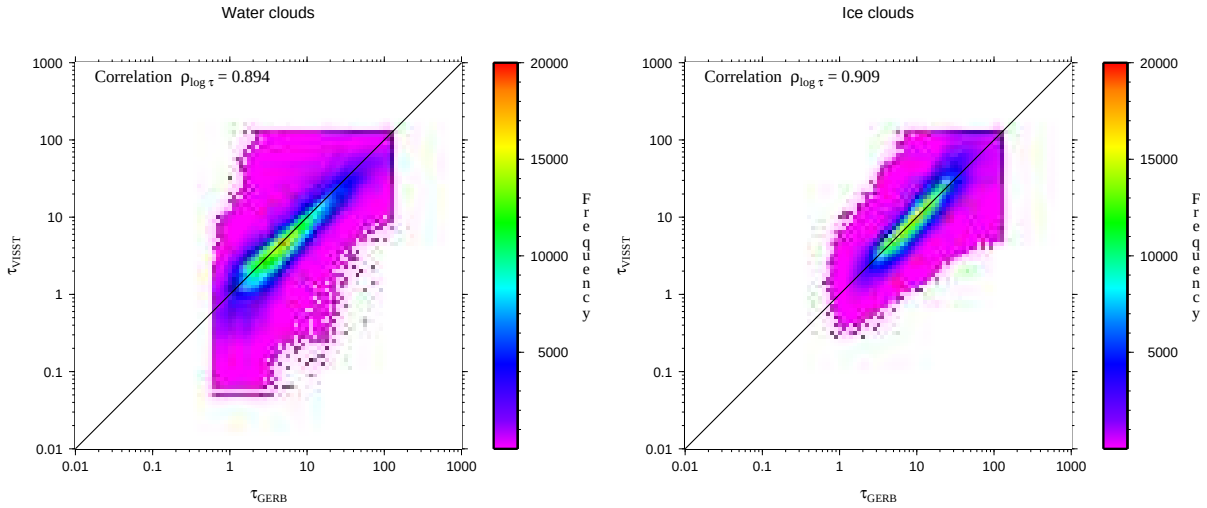

(a) (b)

Figure 6. Frequency histograms of GERB and CERES/VISST cloud optical depth values for (a) water and (b) ice clouds scenes.

have been made with CERES/VISST processing on the same SEVIRI data and results look promising, even if some discrepancies occur. As the VISST processed SEVIRI data reaches an official release status, it is expected that the confidence between both algorithm will further grow. Nevertheless, various factors have already been suggested to explain these discrepancies and further specific investigations are recommended.

Moreover, future works which could result in significant improvements of the GERB scheme will be investigated, such as:

- the use of 1.6 μm SEVIRI channel for better cloud phase discrimination and more specifically for supercooled water clouds,
- the use of thermal channels for thin clouds detection and increase confidence of the cloud detection in the sunglint regions,
- the use of a dynamic surface map according to NDVI and water indexes to cope for surface changes and thus select the most adequate LUT for the cloud optical depth retrieval.

ACKNOWLEDGMENTS

The CERES data were obtained from the NASA Langley Cloud and Radiation Research Group, `http://angler.larc.nasa.gov/satimage/products.html`.

This work was supported by the Research Directorate of the European Commission under contract GERBEC, the Belgian Science Policy Office (BELSPO) under contract PRODEX 5-8 and by European Organisation for the Exploitation of Meteorological Satellites (EUMETSAT) under contract EUMETGERB.

REFERENCES

1. J. Schmetz, P. Pili, S. Tjemkes, D. Just, J. Kerkmann, S. Rota, and A. Ratier, "An introduction to Meteosat second Generation (MSG)," *Bull. Amer. Meteor. Soc.* **83**(7), pp. 977–992, 2002.
2. J. Harries and D. Crommelynck, "The Geostationary Earth Radiation Budget Experiment on MSG-1 and its Potential Applications," *Adv. Space Res.* **24**(7), pp. 915–919, 1999.

3. J. Harries, J. Russel, J. Hanafin, H. Brindley, J. Futyan, J. Rufus, S. Kellock, G. Matthews, R. Wrigley, A. Last, J. Mueller, R. Mossavati, J. Ashmall, E. Sawyer, D. Parker, M. Caldwell, P. Allan, A. Smith, M. Bates, B. Coan, B. Stewart, D. Lepine, L. Cornwall, D. Corney, M. Ricketts, D. Drummond, D. Smart, R. Cutler, S. Dewitte, N. Clerbaux, L. Gonzalez, A. Ipe, C. Bertrand, A. Joukoff, D. Crommelynck, N. Nelms, D. Llewellyn-Jones, G. Butcher, G. Smith, Z. Szewczyk, P. Mlynczak, A. Slingo, R. Allan, , and M. Ringer, "The Geostationary Earth Radiation Budget Project," *Bull. Amer. Meteor. Soc.* **86**, pp. 945–960, 2005.
4. S. Dewitte, L. Gonzalez, N. Clerbaux, A. Ipe, C. Bertrand, and B. De Paepe, "The Geostationary Earth Radiation Budget Edition 1 data processing algorithms," *Adv. Space Res.* **accepted**, 2007.
5. N. Clerbaux, S. Dewitte, L. Gonzalez, C. Bertand, B. Nicula, and A. Ipe, "Outgoing Longwave Flux Estimation: Improvement of Angular Modelling Using Spectral Information," *Remote Sens. Environ.* **85**, pp. 389–395, 2003.
6. N. Clerbaux, S. Dewitte, C. Bertrand, D. Caprion, B. D. Paepe, L. Gonzalez, and A. Ipe, "Angular Dependency Model for the Meteosat Longwave Radiation," *Adv. Space Res.* **submitted**, 2007.
7. B. Wielicki, B. Barkstrom, E. Harrison, R. Lee III, G. Smith, and J. Cooper, "Clouds and the Earth's Radiant Energy System (CERES): An Earth observing system experiment," *Bull. Amer. Meteor. Soc.* **77**, pp. 853–868, may 1996.
8. C. Kummerow, W. Barnes, T. Kozu, J. Shiue, and J. Simpson, "The Tropical Rainfall Measuring Mission (TRMM) Sensor Package," *J. Atmos. Ocean. Tech.* **15**, pp. 809–817, jun 1998.
9. N. Loeb, N. Smith, S. Kato, W. Miller, S. Kupta, P. Minnis, and B. Wielicki, "Angular distribution models for top-of-atmosphere radiative flux estimation from the Clouds and the Earth's Radiant Energy System instrument on the Tropical Rainfall Measuring Mission satellite - Part I: Methodology," *J. Appl. Meteorol.* **42**(2), pp. 240–265, 2003.
10. P. Minnis, D. Young, B. Wielicki, P. Heck, X. Dong, L. Stowe, and R. Welch, "CERES cloud properties derived from multispectral VIRS data," in *Proc. Symp. on Remote Sensing*, pp. 91–102, (Florence, Italy), 1999.
11. P. Minnis, W. Smith, D. Young, L. Nguyen, A. Rapp, P. Heck, and M. Khaiyer, "Near-real-time retrieval of cloud properties over the ARM CART area from GOES data," in *Proc. 12th ARM Science Team Meeting*, p. 7, (St. Petersburg, USA), 2002.
12. N. Loeb, K. Loukachine, N. Smith, B. Wielicki, and D. Young, "Angular distribution models for top-of-atmosphere radiative flux estimation from the Clouds and the Earth's Radiant Energy System instrument on the Tropical Rainfall Measuring Mission satellite - Part II: Validation," *J. Appl. Meteorol.* **42**(12), pp. 1748–1769, 2003.
13. A. Ipe, N. Clerbaux, C. Bertrand, S. Dewitte, and L. Gonzalez, "The gerb edition 1 products seviri scene identification," *IEEE Trans. Geosci. Remote Sens.* **submitted**, 2007.
14. A. Belward, J. Estes, and K. Kline, "The IGBP-DIS 1-km landcover data set DISCover: A project overview," *Photogramm. Eng. Rem. Sens.* **65**(9), pp. 1013–1020, 1999.
15. E. Wolters, R. Roebeling, and A. Feijt, "Quantitative assessment of cloud phase determination from SEVIRI using ground-based cloud radar and lidar," in *Proc. EUMETSAT Meteorological Satellite Conference*, (Helsinki, Finland), 2006.
16. J. Key and A. Schweiger, "Tools for atmospheric radiative transfer: Streamer and FluxNet," *Comp. Geosci.* **24**(5), pp. 443–451, 1998.
17. B. Mayer and A. Kylling, "The libradtran software package for radiative transfer calculations - description and examples of use," *Atmos. Chem. Phys.* **5**, pp. 1855–1877, 2005.
18. C. Cox and W. Munk, "Measurement of the roughness of the sea surface from photographs of the sun's glitter," *J. Opt. Soc. Am.* **44**, pp. 838–850, 1954.
19. T. Nakajima and M. King, "Determination of the optical thickness and effective particle radius of clouds from reflected solar radiation measurements. Part I: Theory," *J. Atmos. Sci.* **47**, pp. 1878–1893, 1990.
20. T. Nakajima and T. Nakajima, "Wide-aera determination of cloud micrpysical properties from NOAA AVHRR measurements for FIRE and ASTEX regions," *J. Atmos. Sci.* **52**, pp. 4043–4059, 1995.
21. A. Ipe, C. Bertrand, N. Clerbaux, S. Dewitte, and L. Gonzalez, "Validation and homogenization of cloud optical depth and cloud fraction retrievals for GERB/SEVIRI scene identification using Meteosat-7 data," *Atmos. Res.* **72**, pp. 17–37, 2004.